Asymmetric Single Graft Block Copolymers: Effect of Molecular Architecture on Morphology

Chin Lee and Samuel P. Gido*

Polymer Science and Engineering Department, W. M. Keck Electron Microscopy Laboratory, University of Massachusetts, Amherst, Massachusetts 01003

Marinos Pitsikalis and Jimmy W. Mays

Department of Chemistry, University of Alabama at Birmingham, Birmingham, Alabama 35294

Nora Beck Tan,† Samuel F. Trevino,† and Nikos Hadjichristidis‡

Polymers Research Branch, U.S. Army Research Laboratory, APG, Maryland 211005-5069, Reactor Radiation Division, NIST, Gaithersburg, Maryland 20899, Department of Chemistry, University of Athens, Panepistimiopolis Zografou 15771, Athens, Greece, and Institute of Electronic Structure and Laser, 711 10 Heraklion, Crete, Greece

Received February 5, 1997; Revised Manuscript Received April 15, 1997[⊗]

ABSTRACT: This paper reports on the synthesis and morphological characterization of graft block copolymers in which a single polystyrene (PS) arm was grafted at an asymmetric position along a polyisoprene (PI) backbone. These materials represent a model series of asymmetric simple graft (ASG) block copolymer structures. The synthesis of these materials was carried out with methods developed for three-arm "miktoarm" star copolymers using anionic polymerization high-vacuum techniques with cholorosilane linking agents. The three arms were two polyisoprene blocks with different degrees of polymerization and one deuterated polystyrene block, which formed an asymmetric simple graft structure (ASG). Molecular characterization was performed using size exclusion chromatography (SEC) with refractive index and UV detection, membrane osmometry, and low-angle laser light scattering. These techniques confirmed that the materials exhibited narrow molecular weight distributions and low compositional heterogeneity. The morphologies formed by these samples were characterized using transmission electron microscopy (TEM) and small-angle neutron scattering (SANS). The ASG structures were compared with structures formed by linear diblock copolymers and other samples having miktoarm structures, like I_2S (symmetric simple graft with PI backbone and one PS branch grafted from the middle) and I_3S (three equal PI arms and one PS arm). Comparisons of the morphologies formed and their dimensions indicated that the chain stretching and lateral crowding due to the miktoarm architecture was partially alleviated by the different lengths of PI blocks in ASG.

Introduction

Diblock copolymer morphological behavior has been mapped by experiments and predicted by theory based on a two-parameter model utilizing volume fraction (ϕ), and χN, the product of the Flory χ parameter and degree of polymerization.[1−6] In the strong segregation limit (large χN), the morphology formed is solely dictated by the relative volume fractions of the respective blocks. Recently, because of a successful strategy to synthesize well-defined miktoarm star block copolymers of the type A_mB_n developed by the group of Hadjichristidis, the molecular architecture was demonstrated experimentally as an additional variable for control of morphology.[7−11]

Connecting different numbers of A and B arms at one junction point (i.e. m not equal to n) creates an asymmetry, due to molecular architecture, in the way that the opposing A and B block materials fill space. Compared to a linear diblock, block materials with two or more arms experience more stretching and more lateral crowding. Additionally, if m and n are not equal, this extra chain stretching will be greater on the side of the interface with a larger number of arms per molecule. To alleviate this asymmetry in chain stretching, there is a shift in interfacial curvature preference: The interface tends to decrease in curvature when viewed from the side of the block material with higher arm number. If the higher arm number occurs on the concave side of the interface, the interface will tend to be less concave than it would be in a linear diblock of the same relative volume fraction. If the higher arm number occurs on the convex side of the interface, then the interfacial curvature will tend to be more convex than it would be in a linear diblock. These curvature preferences, as illustrated in a mean-field morphology diagram calculated by Milner (Figure 1), result in a shift of the morphological transition lines toward higher volume fractions of the lower arm number component. In these calculations, the asymmetry caused by the difference in A and B arm numbers was lumped with the conformational asymmetry inherent in the A and B polymer chains into one asymmetry factor, ϵ. Our previous study of a series of I_2S materials (two polyisoprene arms with equal molecular weight and one polystyene arm) found good agreement with the calculated morphology diagram, except for one sample.[10] The sample at 0.81 PS volume fraction formed a new randomly ordered, worm-like micelle structure, which was demonstrated to be an equilibrium structure by careful annealing experiments.[9] Another series of I_3S materials together with several S_2I and I_2S samples were studied by Tselikas *et al.*[11] These materials

* To whom correspondence should be addressed.
† U.S. Army Research Laboratory and NIST.
‡ University of Athens and Institute of Electronic Structure and Laser.
⊗ Abstract published in *Advance ACS Abstracts,* June 1, 1997.

S0024-9297(97)00172-1 CCC: $14.00

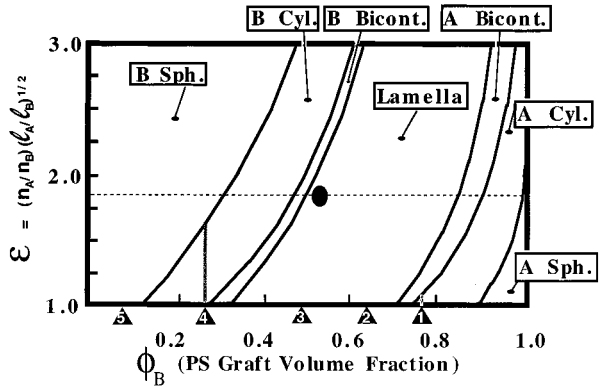

Figure 1. Theoretical phase diagram calculated by Milner. Each triangle represents a specific ASG sample corresponding to the number within the triangle. The oval represents an I_2S sample from ref 11.

showed that Milner's calculation slightly overestimated the degree of shift in morphology boundaries. However, both experiment and theory have demonstrated that miktoarm architecture can have a profound effect on morphology.

In the present paper, a series of three-arm "miktoarm" I_2S block copolymers were synthesized utilizing chlorosilane coupling chemistry.[12] One PI arm is about 3 times longer than the other PI arm. This corresponds to a simple graft structure in which $\tau \approx 0.25$, where τ is the fraction distance along the PI backbone at which the PS graft occurs. The morphology behavior of this asymmetric simple graft structure cannot be predicted directly by Milner's morphology diagram, because the calculation of the ϵ parameter assumes that all blocks of the same type are of the same molecular weight (i.e., $\tau = 0.5$ for the I_2S materials studied previously). In order to generalize the morphology diagram to the asymmetric simple graft structure (ASG), we postulated the following type of relationship in our previous paper:[13] $\epsilon = f(\tau)(l_A/l_B)^{1/2}$. Here, $f(\tau)$ represents the asymmetry due to the architecture, and $(l_A/l_B)^{1/2}$ expresses the conformational asymmetry between the two block materials. l_i (i = A or B) is the ratio of segment volume to the square of statistical segment length for the i block. Since the lateral crowding and additional chain stretching associated with the two chains on one side of the interface in a symmetrically grafted structure ($\tau = 0.5$) should be partially alleviated in the asymmetric simple graft structure, $f(\tau)$ should be between 1 (linear diblock) and 2 (symmetric simple graft architecture, I_2S). The morphology behavior of the five samples presented in this paper basically agreed with this assumption and allows us to place some basic constraints on the form of the $f(\tau)$ relationship.

Experimental Section

Synthesis of Asymmetric Simple Grafts. The asymmetric simple grafts were synthesized by high-vacuum, anionic polymerization in all-glass reactors, provided with breakseals and constrictions for addition of reagents and removal of samples, respectively.[14] All reactors were purged with *n*-butyllithium and rinsed with benzene, which was the solvent for the reactions, prior to introduction of reactants.

The purification of benzene (solvent), styrene-d_8 and isoprene (monomers obtained from Cambridge Isotopes and Aldrich), trichloromethylsilane (linking agent, Aldrich), and methanol (terminating agent) to the standards required for anionic polymerization was performed using reported procedures.[14] The initiator used for all polymerizations, *sec*-butyllithium, was prepared by the reaction of *sec*-butyl chloride (Aldrich) and lithium dispersion (Aldrich) under vacuum and was subsequently diluted with benzene to the concentrations needed for polymer synthesis.

The procedure used for the synthesis of simple grafts, outlined below, is similar to the method adopted by Iatrou and Hadjichristidis[12] for the synthesis of ABC miktoarm star terpolymers.

$$\text{s-BuLi} + \text{Is} \rightarrow \text{PI}_\alpha^-\text{Li}^+$$

$$\underset{\text{(excess)}}{\text{PI}_\alpha^-\text{Li}^+ + \text{CH}_3\text{SiCl}_3} \rightarrow \underset{\text{I}}{\text{CH}_3\text{Si(PI)}_\alpha\text{Cl}_2} + \text{CH}_3\text{SiCl}_3\uparrow + \text{LiCl}$$

$$\text{dS} + \text{s-BuLi} \rightarrow \text{PS}^-\text{Li}^+$$

$$\text{I} + \text{dPS}^-\text{Li}^+ \text{ titration } \text{CH}_3\text{Si(PI)}_\alpha\text{(dPS)Cl} \rightarrow \text{II}$$

$$\text{s-BuLi} + \text{Is} \rightarrow \text{PI}_\beta^-\text{Li}^+$$

$$\underset{\text{(excess)}}{\text{II} + \text{PI}_\beta^-\text{Li}^+} \rightarrow \text{CH}_3\text{Si(PI)}_\alpha\text{(dPS)(PI)}_\beta$$

A dilute solution (ca. 2.5% w/v) of the $PI_\alpha^-Li^+$ solution was reacted with a very large excess of CH_3SiCl_3 (Cl/Li ≅ 100) to avoid coupling. The excess chlorosilane and benzene were removed on the vacuum line. The end-functionalized polymer was then redissolved in pure benzene (distilled through the vacuum line), followed by removal of the solvent under vacuum conditions. After pumping for 1 day, the above procedure was repeated once more, and finally, the product was pumped down for several days at 4 °C. The duration was dependent upon the molecular weight of the sample and the quantity of the linking agent used. Size exclusion chromatography (SEC) analysis of the end-capped specimen (I) showed less than 2% coupling in all cases, usually less than 1%.

In the second step, the dilute (ca. 2.5% w/v) living dPS^-Li^+ solution was added dropwise to a solution of the difunctional linking agent (I). This procedure, called "titration",[12] was monitored visually and via SEC analysis of samples removed from the reaction mixture. This methodology led to the formation of the diblock product with one remaining Si−Cl bond at the junction point (II).

Finally, a small excess of living $PI_\beta^-Li^+$ (ca. 10% w/v), having a molecular weight about one-third that of PI_α chains, was added to the reactor for the preparation of the final product. The excess of $PI_\beta^-Li^+$ was then deactivated with methanol. The product was purified by fractionation involving addition of methanol to dilute solutions (<1% w/v) of the polymer in toluene/hexane mixtures. A small amount of antioxidant (butylated hydroxytoluene) was added to each product.

Polymer Characterization. SEC was conducted in tetrahydrofuran (THF) at 3 °C and a flow rate of 1 mL/min. A set of three Waters Ultrastyragel linear columns was used, with a Waters Model 510 pump, a Waters Model 410 differential refractometer, and a LDC/Milton Roy variable wavelength UV detector. The UV response was calibrated with solutions of polystyrene standards so that SEC could be utilized to examine both the molecular weight distributions and compositions of the copolymers.

Weight-average molecular weights (M_w) and second virial coefficients (A_2) were measured with a Chromatix KMX-6 low-angle laser light scattering (LALLS) photometer. This instrument, equipped with a He−Ne laser, operates at a wavelength of 633 nm. THF, purified by refluxing over sodium followed by distillation, was used as the solvent at 2 °C. The data analysis involved plots of $(Kc/\Delta R_\theta)$ versus c, where K is an optical constant, c is the polymer concentration, and ΔR_θ is the excess Rayleigh ratio. Refractive index increments (dn/dc) were measured under the same conditions using an Otsuka DRM-1020 differential refractometer, which was calibrated with NaCl solutions.

Number-average molecular weights (M_n) and A_2 values were measured with a Jupiter Instruments Co. membrane osmometer at 38 °C. Toluene, distilled over CaH_2, was the solvent.

Table 1. Molecular Characteristics of the Asymmetric Simple Grafts and Their Component Segments

sample	$10^{-4}M_n$[a] PI$_\alpha$	10^3A_2[a]	$10^{-4}M_n$ dPS	$10^{-4}A_2$[a]	$10^{-4}M_n$[a] PI$_\beta$	10^3A_2	$10^{-4}M_n$ star	10^4A_2[a]	$10^{-4}M_w$[b] star	10^4A_2[b]	% wt dPS$_c$
ASG-1	1.27[b]	2.90[b]	9.06	6.02	0.36[d]		11.7	5.74	11.8	6.06	80.1
ASG-2	2.37	1.79	5.67	4.19	0.61[d]		8.44	7.04	9.38	7.39	67.4
ASG-3	3.39	1.61	5.05	6.06	1.05	2.25	9.34	7.17	9.96	7.75	51.5
ASG-4	5.45	1.26	2.79	9.16	1.39	2.17	9.23	9.36	9.67	10.3	29.1
ASG-5	9.69	1.18	1.52[b]	9.97[b]	3.10	1.69	13.5	7.20	13.9	10.8	10.1

[a] By membrane osmometry. [b] M_w by LALLS. [c] By UV−SEC. [d] By VPO.

Regenerated cellulose and cellulose acetate membranes were used for the measurements. Square root plots of π/c versus c, where π is the osmotic pressure, were used in all cases. For samples with molecular weights smaller than about 10 000, a UIC Model 070 vapor pressure osmometer was used at 40 °C with benzene, distilled over CaH_2, as solvent. Instrumental calibration was performed using benzil.

Morphological Characterization. Solid films approximately 2 mm thick of graft block copolymers were slowly cast from 5 weight % polymer solutions in toluene, a nonpreferential solvent. Casting was performed at room temperature, and evaporation of solvent was controlled to form a solid film after 10−14 days. The films were given several more days at room temperature and atmospheric pressure and an additional several days under high vacuum at room temperature in order to remove residual solvent. The samples were then annealed for 1 week under high vacuum at 120 °C in order to further promote the approach to an equilibrium structure.

After annealing, samples for electron microscopy were microtomed in a Leica Ultracut cryoultramicrotome. Sections approximately 50−100 nm thick were cut with a Diatome diamond knife at a sample temperature of −110 °C and a knife temperature of −90 °C. The sections were stained in OsO_4 vapors for 4 h. Transmission electron microscopy (TEM) was performed on a JEOL 100CX operated at 100 kV accelerating voltage. Small-angle neutron scattering (SANS) was performed on beam line NG3 at the Cold Neutron Research Facility of the National Institute of Standards and Technology in Gaithersburg, MD. The NG3 instrument uses pinhole collimation of the monochromated beam. Data were recorded with the incident neutron radiation striking the sample parallel to the surface of the cast films at a wavelength of 5 Å and at sample to detector distances (camera lengths) of both 3 and 13 m. Small-angle X-ray scattering (SAXS) was also performed using a sealed tube Cu Kα source, pinhole collimation, and film (Kodak DEF-5) as a detector.

Results

Molecular Characterization. Molecular characteristics of the asymmetric simple graft copolymers are summarized in Table 1. There is close agreement (within experimental error) in all cases between the measured compositions and those expected on the basis of absolute molecular weight measurements on the component segments of the graft copolymers. Although not shown in Table 1, SEC polydispersity measurements yielded M_w/M_n values ranging from 1.04 to 1.06 for all of the ASG copolymers. The M_w and M_n values in Table 1 were obtained using LALLS and membrane osmometry, respectively. Taking the ratios of the M_w and M_n values given in the table yields polydispersities for some samples outside the range measured by SEC. This most likely is a result of small systematic errors in the LALLS and membrane osmometry measurements of the molecular weights. SEC provides a more reliable means to measure polydisperity since M_w and M_n are both obtained by the same method and thus systematic errors cancel out of their ratio. The present findings, combined with previous work on the synthesis of symmetrical simple grafts,[10,15,16] demonstrate that it is now possible to place a single "graft", of predetermined length, at virtually any point along the polymer backbone. This method is presently limited to the range of monomers that undergo controlled anionic polymerization and reaction with chlorosilane linking agents.

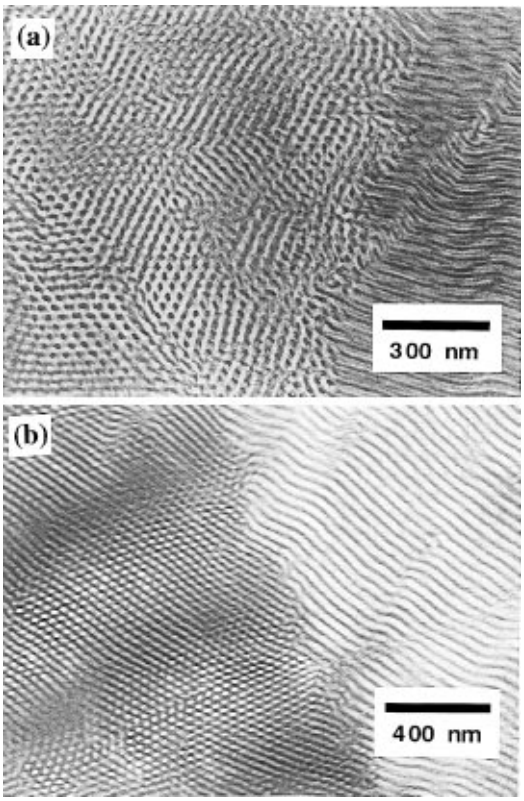

Figure 2. TEM images of the cylinder morphologies of samples ASG-1 (a) and ASG-4 (b).

Morphology. TEM images of the asymmetric simple graft block copolymer morphologies are shown in Figures 2−4, and the SANS results on these materials are shown in Figures 5 and 6, which have sample to detector distances (camera lengths) of 3 and 13 m respectively. The SANS results for each sample are displayed as a one-dimensional plot of intensity (I) vs scattering vector (q), integrated radially from a two-dimensional scattering pattern. We define q^* as the scattering vector of the Bragg peak with the lowest scattering angle and q_n as the series of Bragg peaks, in order of increasing scattering angle, beginning with q^*. The ratios of q_n/q^* for each peak are indicated in Figures 5 and 6. On the basis of the TEM image in Figure 2a and the SANS data in Figure 5a, we assign sample ASG-1 a morphology of hexagonally packed PI cylinders in a PS matrix. The TEM image shows both hexagonal, end-on, and side-on projections of the cylindrical structure, and the SANS pattern for ASG-1 contains two peaks with q_n/q^* ratios of 1 and $\sqrt{3}$, corresponding to the {10} and {11} sets of planes, respectively, in the hexagonal structure.

Both ASG-2 and ASG-3 yield PI−PS lamellar structures, as shown in the TEM images of Figure 3a,b. Both of the I vs q plots in Figure 6 show 5 orders of reflection

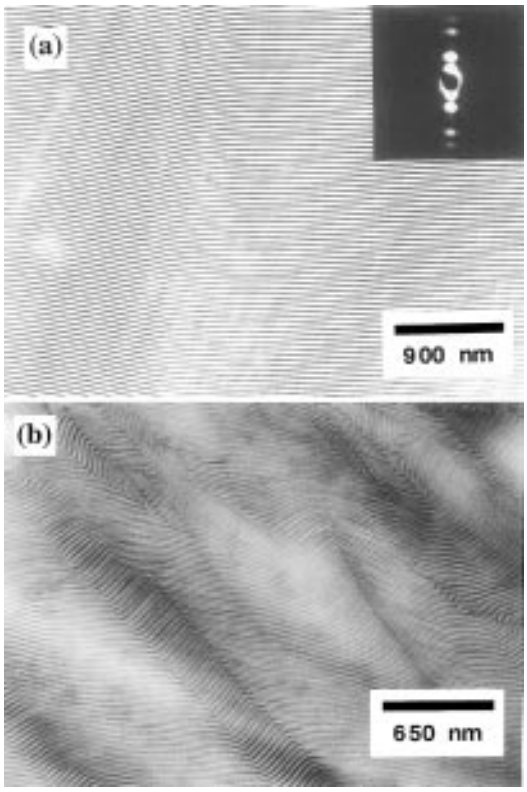

Figure 3. TEM images of the lamellar morphologies of samples ASG-2 (a) and ASG-3 (b). A SAXS pattern from ASG-2 is inset in (a).

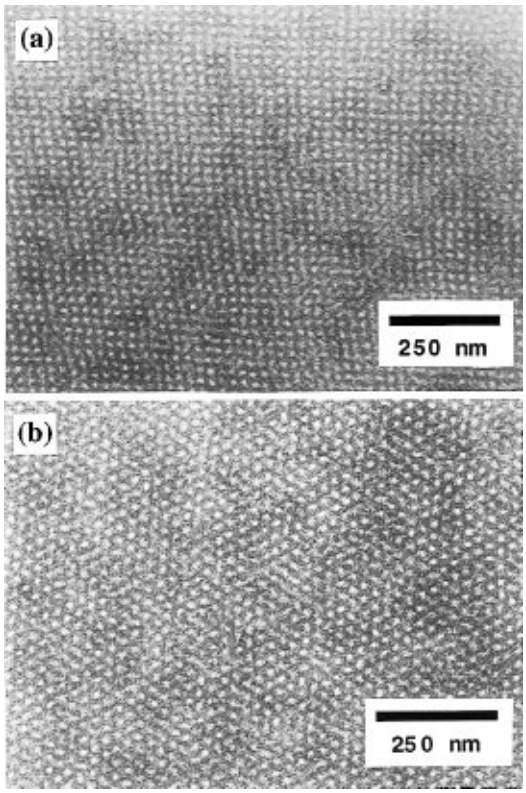

Figure 4. TEM images of the spherical morphology of sample ASG-5. Both a [100] projection (a) and a [111] projection (b) are shown.

at q^*, $2q^*$, $3q^*$, $4q^*$, and $5q^*$. A two-dimensional SAXS pattern of ASG-2 is inset in the TEM micrograph shown in Figure 3a. Both this pattern and the image show the unusual long-range order of ASG-2. In the SAXS pattern the concentration of scattered intensity is along

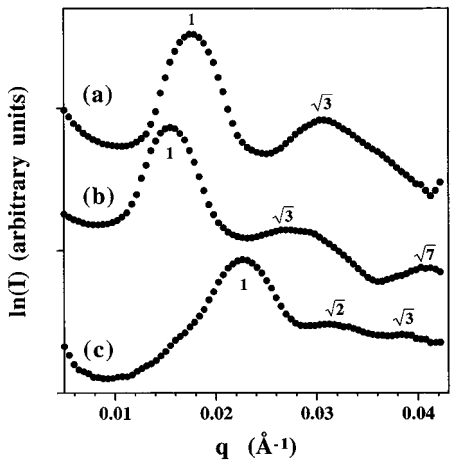

Figure 5. SANS intensity, I, vs scattering vector, q, for ASG-1 (a), ASG-4 (b), and ASG-5 (c), at 3 m camera length.

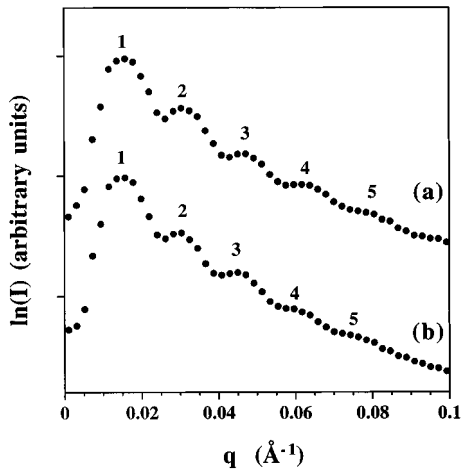

Figure 6. SANS intensity vs scattering vector for ASG-2 (a) and ASG-3 (b), at 13 m camera length.

the equator with essentially no arcs extending azimuthally, indicating that the lamellar layers are predominantly parallel with the surface of the film. Due to the convolution of the third Bragg peak ($q_3 = 0.47$) and the second minimum of the form factor for the polystyrene lamellar domain (at $q = 0.48$), this Bragg peak is missing in the SAXS pattern. However, the third Bragg peak still shows up in the one-dimensional SANS pattern in Figure 6a. This may be due to the higher dispersity of wavelength and poorer collimation inherent in the SANS experiment, which smears out the minimum in the form factor. With the exception of the third peak, both SAXS and SANS give the same values of q at scattering maxima for ASG-2. ASG-3 displays a much higher degree of grain misorientation in its structure than ASG-2, as revealed by TEM and by the isotropic ring patterns obtained in SANS.

The TEM image of ASG-4, in Figure 2b, shows hexagonally packed PS cylinders in a PI matrix. Both hexagonal, end-on, and side-on projections of the cylinder structure are visible. The SANS I vs q plot for ASG-4, Figure 5b, shows three peaks with q_n/q^* ratios of 1, $\sqrt{3}$, and $\sqrt{7}$, corresponding to the {10}, {11}, and {21} families of planes. The second peak has a very long and rough tail, which may indicate that the reflection with q_n/q^* of 2 from the {20} family of planes is hidden under this peak. ASG-5 formed a cubic array of PS spheres in a matrix of PI. Both a 4-fold [100] projection and a hexagonal [111] projection of the cubic structure are

Table 2. ASG Morphology Characteristics

sample	ϕ_s	t	R^a (Å)	morphology
ASG-1	0.75	0.22	410	hexagonally packed PI cylinders in a PS matrix
ASG-2	0.62	0.20	405	alternating PS and PI lamellae
ASG-3	0.46	0.24	419	alternating PS and PI lamellae
ASG-4	0.25	0.20	353	hexagonally packed PS cylinders in a PI matrix
ASG-5	0.08	0.24	273	cubic array PS spheres in PI matrix

[a] $R = 2\pi/q^*$, where $q^* = 4\pi/\lambda(\sin\theta_l)$ and θ_l is the scattering angle for the lowest angle Bragg peak; corresponds to $d_{(10)}$ for hexagonally packed cylinders, $d_{(100)}$ for lamellae, and either $d_{(100)}$ or $d_{(110)}$ for simple cubic or body-centered cubic, respectively.

Table 3. Comparison of Lattice Dimensions of Linear Diblock, ASG, I_2S, and I_3S

	ϕ_s	M_n	R (Å)	$(RV^{-2/3}/(RV^{-2/3})_{linear})_{exp}$	$(RV^{-2/3}/(RV^{-2/3})_{linear})_{cal}$	ref
I_{3S}	0.61	94 400	380	0.62	0.64	11
I_{2S}	0.62	83 000	390	0.72	0.79	10
ASG-2	0.62	84 400	405	0.74	0.89	
linear	0.56	105 000	660	1	1	19

shown in Figure 4a,b. Figure 5c shows the SANS pattern of ASG-5 with three peaks. The q_n/q^* ratios of 1, $\sqrt{2}$, and $\sqrt{3}$ of these three peaks are consistent with both body-centered cubic (110, 200, and 211 for bcc) and simple cubic (100, 110, and 111 for sc) symmetries. The morphology results on the asymmetric simple graft materials are summarized in Table 2.

Discussion

A linear chain of a lamella-forming diblock can be thought of as contained in a rectangular box or *wedge*,[8] which has dimensions optimized to give the minimum free energy. If we cut the A block into two equal lengths and still graft both pieces to the junction point at the interface, forming an I_2S molecule, the shorter A chains must stretch twice as long, on average, to fill space to constant density. The increased stretching energy of the A chains can be relaxed by compressing the wedge normal to the interface (which must be paid for by an increase in interfacial area) and/or by changing the wedge shape (and thus changing the morphology), for instance by curving the interface away from the crowded A blocks. Here we combine the results of the current study with our previous results[13] and published results on miktoarm block copolymers in order to draw conclusions regarding the effect of molecular architecture on microdomain dimension and morphological transitions.

The lattice dimensions of a linear diblock copolymer, an I_2S, and an I_3S material all with the same composition, molecular weight, and the same morphology should decrease sequentially, because of the increase in the stretching energy of the PI blocks. Of course, such materials may also change their morphologies to structures with greater interfacial curvature away from the multiple PI blocks. However, if the series of materials were to remain in the same type of morphology the increased chain stretching with increasing PI arm number would lead to progressively larger interfacial area per chain and a smaller dimension normal to the interface.[17] Here we will compare the lattice dimensions for diblock, ASG, I_2S, and I_3S materials of similar molecular weight and composition, all of which form lamellar morphologies. Such comparisons were not possible for other morphologies since we could not find samples of all four molecular architectures with similar compositions and the same type of morphology.

From Milner's strong segregation calculation, the average single-chain dimension normal to the interface, R (half of the long period), for lamella with minimum free energy is

$$RV^{-2/3} = \left(\frac{4\gamma}{\pi^2}\right)^{1/3}(n_A n_B)^{-1/3}(l_A l_B)^{-1/6}[\epsilon(1-\phi_A) + \phi_A/\epsilon]^{-1/3} \quad (1)$$

where $\epsilon = (n_A/n_B)(l_A/l_B)^{1/2}$ and $l_i = v_i/b_i^2$. Here γ is the interfacial energy. As with linear diblocks in strong segregation, R scales as the 2/3 power of the chain volume, V, or the degree of polymerization, N. Thus if the strong segregation assumption remains valid, the product $RV^{-2/3}$ is a molecular weight independent measure of domain size. R has a slight volume fraction (ϕ_A) dependence and decreases as the asymmetry factor, ϵ, increases. The asymmetry depends on two factors, molecular architecture (the ratio of the number of A and B arms, n_A and n_B) and the chain statistics of two types of blocks (segment volume, v_i, and statistical segment length, b_i). The asymmetry from molecular architecture is our main concern here; however, there is a slight asymmetry inherited in different chain statistics and the packing density of PI and PS,[10] which causes the $(l_A/l_B)^{1/2}$ to be 0.89.

We list the data for linear diblock PS−PI copolymer, I_2S, and I_3S from refs 19, 10, and 11 and our ASG-2 in Table 3. All these samples formed alternating PS-PI lamellar structures. In order to isolate the effect of architecture, we have chosen these samples to have similar overall compositions (volume fractions) and molecular weights. The fifth and sixth columns in Table 3 are the ratios of $RV^{-2/3}$ for the miktoarm copolymer to the value for the linear diblock copolymer, calculated from the experimental data and from eq 1, respectively. These $(RV^{-2/3})/(RV^{-2/3})_{linear}$ ratios decrease with increasing junction point functionality in the sequence linear diblock PS−PI, I_2S, and I_3S. Equation 1 resulted in fairly good predictions, but still some differences exist between the experimental and calculated dimensions. The differences may be caused by experimental error (as indicated by the diversity of data in the literature) or by the approximations inherent in the theory. Here we assumed all the samples have high enough molecular weight to be in the strong segregation region, and $V^{-2/3}$ is used to normalize for the molecular weight differences among the samples. Since all the samples have similar molecular weights (between 80K and 105K), any slight deviation from the SSL should not significantly affect the relative values of $RV^{-2/3}$.

The $(RV^{-2/3})/(RV^{-2/3})_{linear}$ ratio of ASG-2 to linear diblock copolymer is also given in Table 3. Its value is between those of the linear diblock copolymer and the

I_2S symmetric simple graft, i.e. the lateral crowding and chain stretching on the PI side of the interface is partially alleviated in the asymmetric-grafted structure. The calculation of the dimensions of the microdomains in asymmetric simple grafts was not considered in Milner's calculation. But we can easily use the bimodal brush concept[18] to modify eq 1. Starting from eq 11 in ref 18, we can get eq 2 for the lamellar dimension of the asymmetric-grafted structure with minimum free energy, where τ is the fraction distance along the PI backbone at which the PS graft occurs.

$$RV^{-2/3} = \left(\frac{4\gamma}{\pi^2}\right)^{1/3}(l_A l_B)^{-1/6}[\epsilon_{linear}(1-\phi_A)(1+6\tau) + \phi_A/\epsilon_{linear}]^{-1/3} \quad (2)$$

Here $\epsilon_{linear} = (l_A/l_B)^{1/2}$ and $0 \le \tau \le 0.5$. At $\tau = 0$ and 0.5, eq 2 gives the results for linear diblock copolymer and I_2S, respectively. Equation 2 shows that $RV^{-2/3}$ decreases with increasing τ from 0.0 to 0.5. The value of τ for ASG-2 is about 0.2, and we also list the calculated result from eq 2 in Table 2. The experimental and calculated $RV^{-2/3}$ results for the ASG both show the expected trend, falling between the linear diblock and I_2S dimensions. However, there is some discrepancy between the actual experimental and calculated values which again might be attributed to experimental uncertainty or to inaccuracies in the theoretical approximations.

All five asymmetric grafted samples in this study show the same morphology as their linear diblock analogues. These five samples were mapped onto the morphology diagram, Figure 1. However, the asymmetric factors, ϵ, are not known for the ASG samples; thus we put a vertical bar for each ASG sample crossing possible values of ϵ on the diagram. In constructing these bars it was assumed that the asymmetry factor for an ASG structure is between that of a linear diblock and that of a symmetric simple graft, I_2S, i.e. $0.89 < \epsilon < 1.78$. ASG-1, with 75 vol % of PS, shows a morphology of hexagonally packed PI cylinders in a PS matrix. This constrains ϵ to a very small range of values, indicated by the small bar on the diagram. Sample ASG-2, which was used in the comparison of lamellar dimensions across different architectures, does not allow us to place any constraints on ϵ since at this composition the predicted structure is lamellar across the whole range from 0.89 to 1.78.

According to Milner's calculation, the composition of ASG-3, 46 vol %, would give both I_2S and linear diblock copolymers the same lamellar morphology. However, there is an I_2S sample with 53 vol % from the study of Tselikas et al.[11] that forms a bicontinuous morphology. The position of his sample is also plotted in Figure 1. Regardless of the discrepancy between the theoretical morphology prediction (lamella) and the experimental result, the fact that the Tselikas sample is bicontinuous may indicate that ASG-3 behaves in a manner that is intermediate between I_2S and linear diblock copolymers. ASG-4 has a morphology of hexagonally packed PS cylinders in a PI matrix, which constrains the ϵ value of this sample to be less than 1.58. Otherwise, the material would form spheres. The last sample, ASG-5, forms a morphology with spherical PS domains in a PI matrix. No bar is shown on the morphology diagram since at this composition I_2S and linear diblock copolymer would both give this spherical morphology.

As discussed in our previous work,[13] if ϵ for an asymmetric grafted structure is assumed to be a function of τ and this function is the same for all morphology transition lines on the diagram, then bounds on this function could be obtained from the bars in Figure 1. In the definition of ϵ, the ratio of the arm numbers is replaced by the function $f(\tau)$: $\epsilon = f(\tau)(l_A/l_B)^{1/2}$. Thus, $f(\tau)$ is calculated by dividing ϵ by $(l_A/l_B)^{1/2}$, which is 0.89 for PS−PI block copolymers. This conversion allows the mapping of the bars in Figure 1 onto an $f(\tau)$ vs τ plot in Figure 7. There is an extra bar in Figure 7 that was obtained from our work on the "π" architecture.[13] The bars in Figure 7 suggest that there may be an inflection point of $f(\tau)$ between $\tau = 0.2$ and $\tau = 0.3$. More data would be necessary to fully describe this function. However, the scant data we have indicates that for τ close to zero, the system behaves like a diblock. As τ increases, the behavior changes rapidly in the range $0.20 < \tau < 0.35$ from diblock-like to symmetric simple graft-like behavior. As the smaller of the two arms in the ASG structure increases in length, in this transition range, the two blocks begin to crowd each other and stretch more normal to the interface.

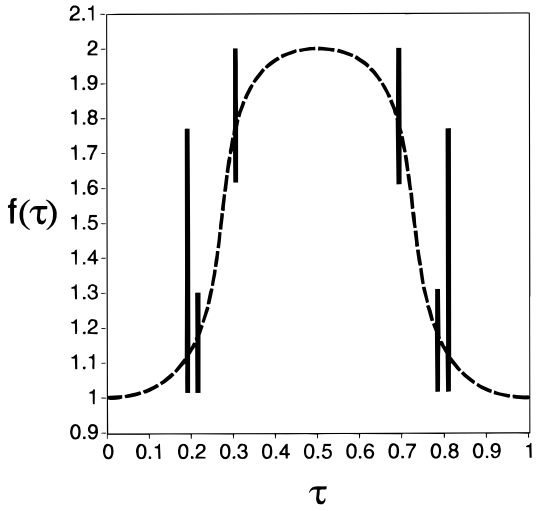

Figure 7. Possible $f(\tau)$ relationship. Bold vertical bars represent allowable ranges of $f(\tau)$ values.

Conclusions

Block copolymers with asymmetric simple graft (ASG) architectures were synthesized using anionic polymerization and chlorosilane linking. These molecules were characterized using size exclusion chromatography, membrane osmometry, and low-angle laser light scattering. This characterization work confirmed the desired molecular architectures and narrow molecular weight distributions, thus demonstrating that it is now possible to place a single "graft", of predetermined length, at virtually any point along the polymer backbone.

The morphologies of these samples were characterized using TEM and SANS. The results were compared with the morphology behavior of linear diblock copolymers and I_2S and I_3S polymers from the literature. Although all the ASG samples showed the same morphology as their linear diblock analogues, we can still observe the effect of the miktoarm architecture by comparing lattice dimensions of samples with different architectures but similar compositions and degrees of polymerization. The lattice dimensions decrease in the sequence of linear diblock, ASG, I_2S, and I_3S, which is qualitatively consistent with Milner's calculation. Both comparison of morphology and lattice dimension indicate that the

asymmetric simple graft structure does partially alleviate the chain stretching and lateral crowding of the two PI chains per molecule from the condition in the symmetric simple graft structure, I_2S. To demonstrate this effect, we postulated a general relationship between the molecular asymmetry parameter, ϵ, and the fractional location of the graft along the backbone, τ.

Acknowledgment. J.W.M., M.P., and S.P.G. acknowledge funding from the U.S. Army Research Office (ARO) under contract DAAH04-94-G-0245. S.P.G. acknowledges ARO funding through an Army Young Investigator Award DAAH04-95-1-0305. We acknowledge the use of the TEM instrument in the W. M. Keck Polymer Morphology Laboratory at the University of Massachusetts Amherst, ARO instrumentation funding (DAAH04-95-1-0005), and Central Facility Support from the Materials Research Science and Engineering Center (MRSEC) at the University of Massachusetts Amherst. We also acknowledge the staff of the Cold Neutron Research Facility at NIST for assistance with SANS experiments. N.H. wishes to acknowledge the Greek General Secretariate of Research and Technology for financial support.

References and Notes

(1) Leibler, L. *Macromolecules* **1980**, *13*, 1602.
(2) Helfand, E.; Wasserman, Z. R. In *Microdomain Structure and the Interface in Block Copolymers*; Goodman, I.; Ed.; Elsevier Applied Science Publisher: London, 1982; Vol. 1, Chapter 5, p 99.
(3) Semenov, A. N. *Sov. Phys. JETP* **1985**, *61*, 733.
(4) Forster, S.; Khandpur, A. K.; Zhao, J.; Bates, F. S.; Hamley, I. W.; Ryan, A. J.; Bras, W. *Macromolecules* **1994**, *27*, 6922.
(5) Khandpur, A. K.; Forster, S.; Bates, F. S.; Hamley, I. W.; Ryan, A. J.; Bras, W.; Almdal, K.; Mortensen, K. *Macromolecules* **1995**, *28*, 8796.
(6) Matsen, M. W.; Bates, F. S. *Macromolecules* **1996**, *29*, 1091.
(7) Hadjichristidis, N.; Iatrou, H.; Behal, S. K.; Chludzinski, J. J.; Disko, M. M.; Garner, R. T.; Liang, K. S.; Lohse, D. J.; Milner, S. T. *Macromolecules* **1993**, *26*, 5812.
(8) Milner, S. T. *Macromolecules* **1994**, *27*, 2333.
(9) Pochan, D. J.; Gido, S. P.; Pispas, S.; Mays, J. W. *Macromolecules* **1996**, *29*, 5099.
(10) Pochan, D. J.; Gido, S. P.; Pispas, S.; Mays, J. W.; Ryan, Anthony J.; Fairclough, J. Patrick A.; Hamley, Ian W.; Terrill, Nicholas J. *Macromolecules* **1996**, *29*, 5091.
(11) Tselikas, Y.; Hadjichristidis, N.; Iatrou, H.; Liang, K. S.; Lohse, D. J. *J. of Chem. Phys.* **1996**, *105*, 2456.
(12) Iatrou, H.; Hadjichristidis, N. *Macromolecules* **1992**, *25*, 4649.
(13) Gido, S. P.; Lee, C.; Pochan, D. J.; Pipas, S.; Mays, J. W.; Hadjichristidis, N. *Macromolecules* **1996**, *29*, 7022.
(14) Morton, M.; Fetters, L. J. *Rubber Chem. Technol.* **1975**, *48*, 359.
(15) Mays, J. W. *Polym. Bull.* **1990**, *23*, 247.
(16) Iatrou, H.; Siakali-Kioulafa, E.; Hadjichristidis, N.; Roovers, J.; Mays, J. W. *Polym. Sci., Polym. Phys. Ed.* **1995**, *33*, 1925.
(17) Beyer, F. L.; Gido, S. P.; Poulos, Y.; Avgeropoulos, A.; Hadjichristidis, N. *Macromolecules*, submitted for publication.
(18) Milner, S. T.; Witten, T. A.; Cates, M. E. *Macromolecules* **1989**, *23*, 853.
(19) Hashimoto, T.; Nagatoshi, K.; Todo, A.; Hasagawa, H.; Kawai, H. *Macromolecules* **1974**, *7*, 364.

MA970172P